Otting, G., Senn, H., Wagner, G., & Wüthrich, K. (1986) *J. Magn. Reson. 70*, 500–505.
Piantini, U., Sørensen, O. W., & Ernst, R. R. (1982) *J. Am. Chem. Soc. 104*, 6800–6801.
Rance, M., Sørensen, O. W., Bodenhausen, G., Wagner, G., Ernst, R. R., & Wüthrich, K. (1983) *Biochem. Biophys. Res. Commun. 117*, 479–485.
Shaka, A. J., & Freeman, R. (1983) *J. Magn. Reson. 51*, 169–173.
Shaka, A. J., Keeler, J., Frenkiel, T., & Freeman, R. (1983) *J. Magn. Reson. 52*, 335–338.
Smillie, R. M. (1965) *Biochem. Biophys. Res. Commun. 20*, 621–629.
Smith, W. W., & Ludwig, M. L. (1974) *J. Biol. Chem. 249*, 4383–4392.
Smith, W. W., Burnett, R. M., Darling, G. D., & Ludwig, M. L. (1977) *J. Mol. Biol. 117*, 195–225.
Smith, W. W., Pattridge, K. A., Ludwig, M. L., Petsko, G. A., Tsernoglou, D., Tanaka, M., & Yasunobu, K. T. (1983) *J. Mol. Biol. 165*, 737–755.
Stockman, B. J., Westler, W. M., Mooberry, E. S., & Markley, J. L. (1988) *Biochemistry 27*, 136–142.
Stockman, B. J., Reily, M. D., Westler, W. M., Ulrich, E. L., & Markley, J. M. (1989) *Biochemistry 28*, 230–236.
Stockman, B. J., Krezel, A. M., Markley, J. L., Leonhardt, K. G., & Straus, N. A. (1990) *Biochemistry 29*, 9600–9609.
Tollin, G., & Edmondson, D. E. (1980) *Methods Enzymol. 69*, 392–406.
Vervoort, J., Muller, F., Mayhew, S. G., van den Berg, W. A. M., Moonen, C. T. W., & Bacher, A. (1986) *Biochemistry 25*, 6789–6799.
Wagner, G., & Zuiderweg, E. R. P. (1983) *Biochem. Biophys. Res. Commun. 113*, 854–860.
Watenpaugh, K. D., Sieker, L. C., & Jensen, L. M. (1973) *Proc. Natl. Acad. Sci. U.S.A. 70*, 3857–3860.
Watt, W., Tulinsky, A., Swenson, R. P., & Watenpaugh, K. D. (1991) *J. Mol. Biol.* (in press).
Wüthrich, K. (1986) *NMR of Proteins and Nucleic Acids*, Wiley, New York.
Wüthrich, K., Billiter, M., & Braun, W. (1984) *J. Mol. Biol. 180*, 715–740.
Zuiderweg, E. R. P., & Fesik, S. W. (1989) *Biochemistry 28*, 2387–2391.

Two- and Three-Dimensional Proton NMR Studies of Apo-Neocarzinostatin

Xiaolian Gao* and William Burkhart

Structural and Biophysical Chemistry, Glaxo Research Institute, 5 Moore Drive, Research Triangle Park, North Carolina 27709

Received February 26, 1991; Revised Manuscript Received April 25, 1991

ABSTRACT: Neocarzinostatin (NCS) is an antitumor protein from *Streptomyces carzinostaticus* that is identical in apo-protein sequence with mitomalcin (MMC) from *Streptomyces malayensis*. We describe the use of apo-NCS as a model system for applying combined two- and three-dimensional (2D and 3D) proton NMR spectroscopy to the structure determination of proteins (M_r > 10K) without isotope labeling. Strategies aimed at accurately assigning overlapped 2D cross-peaks by using semiautomated combined 2D and 3D data analysis are developed. Using this approach, we have assigned 99% of the protons, including those of the side chains, and identified about 1270 intra- and interresidue proton–proton interactions (fixed distances are not included) in apo-NCS. Comparing our results with those reported recently on 2D NMR studies of apo-NCS [Adjadj, É., Mispelter, J., Quiniou, É., Dimicoli, J.-L., Favadon, V., & Lhoste, J.-M. (1990) *Eur. J. Biochem. 190*, 263–271; Remerowski M. L., Glaser, S. J., Sieker, L., Samy, T. S. A., & Drobny, G. P. (1990) *Biochemistry 29*, 8401–8409] demonstrated advantages of proton 3D NMR spectroscopy in protein spectral assignments. We are able to obtain more complete proton resonance and secondary structural assignments and find several misassignments in the earlier report. Strategies utilized in this work should be useful for developing automation procedures for spectral assignments.

Several considerations have contributed to the initiation of the studies of antitumor proteins mitomalcin (MMC) and neocarzinostatin (NCS) isolated from various species of *Streptomyces* (Ishida et al., 1965; McBride et al., 1965). Actinoxanthin and auromomycin are the other two members known to this antitumor protein family (Montgomery et al., 1981). MMC, NCS, and auromomycin are structurally interesting. Each of these proteins is believed to contain a nonprotein component noncovalently bound to the apoprotein, which presumably protects the labile nonprotein molecule from decomposition in aqueous solution (Napier et al., 1979; Suzuki et al., 1980; Montgomery et al., 1981; Naoi et al., 1982). These ligand–protein complexes are important models for understanding fundamental aspects of specific molecular recognition between ligands and protein host molecules. The nonprotein component in NCS has been well characterized in solution (Goldberg, 1986; Myers et al., 1988). It contains a highly active diynene cyclic moiety and was shown to cause chain cleavage along the DNA backbone (Lee & Goldberg, 1989; Jung & Kohnlein, 1981). However, information about the identities and structures of the nonprotein components in apoproteins other than NCS and the mechanisms of the in vivo antitumor activities are still lacking. Progress in this area is awaiting high-resolution structural information for both apo- and holoproteins. High-resolution crystal structures of actinoxanthin and apo-auromomycin have been reported (Pletnev

0006-2960/91/0430-7730$02.50/0

et al., 1982; Roey & Beerman, 1989).

In addition to the interest in solving the structures of these antitumor proteins, it appears that this family of proteins is of suitable size (~11 kDa) for developing homonuclear multidimensional NMR applications for the high-resolution structure determinations of macrobiomolecules without isotope labeling.

Multidimensional NMR spectroscopy has been recently shown to be a powerful tool for elucidating high-resolution three-dimensional structures of biologically important macromolecules (Griesinger et al., 1987, 1989; Kay et al., 1990; Fesik & Zuiderweg, 1990). Heteronuclear 3D NMR spectroscopy correlates ^1H with other nuclei, such as ^{13}C and ^{15}N, providing assistance in assigning overlapped proton resonances and the information about the torsional angles along the peptide backbones. Homonuclear 3D NMR spectroscopy detects the interactions between nuclear resonances of the same type, such as protons, greatly enhancing the resolution of 2D spectra (Vuister et al., 1988, 1989, 1990). Heteronuclear 3D NMR experiments take advantage of well-resolved chemical shifts of ^{13}C or ^{15}N to achieve the assignments of overcrowded proton resonances. However, these types of experiments require isotopically labeled material, restricting its applications in certain circumstances. Homonuclear 3D NMR spectroscopy, on the other hand, does not require specially prepared sample. Its potential has been demonstrated by recent studies of various biomolecules (Vuister et al., 1989, 1990; Breg et al., 1990; Padilla et al., 1990). A major advantage of a 3D NMR data set is the simplicity of the spectrum: in replacing a 2D NMR spectrum that contains a large number of overlapped cross-peaks, each of the planes in a 3D data set gives much fewer cross-peaks, and thus, the cross-peaks in the planes of a 3D data set are better defined than their counterparts in a 2D data set. Assignment strategies of the homonuclear 3D NMR spectra based on sequential proton–proton connectivities have been demonstrated (Vuister et al., 1990). However, the aspect of applying 3D data to resolve 2D spectral ambiguities has not been fully addressed.

In this work, we have used proton 2D and 3D NMR techniques as complementary tools to study the structure of apo-NCS. Our emphasis in analyzing 3D data is to develop strategies resolving ambiguities existing in 2D data. Specifically, in the process of data analyses, we have tried to answer questions, such as what unique information 3D NMR data can offer and how such specific information can be extracted. We found that 3D proton NMR compliments 2D data well and is a necessary tool for the de novo high-resolution structure determinations of proteins of apo-NCS size (M_r > 10K). As this work was in progress, proton assignments and secondary structure of apo-NCS were reported on the basis of 2D NMR studies (Adjadj et al., 1990; Remerowski et al., 1990). This provided an opportunity for directly comparing our results with those obtained without utilizing 3D data (Adjadj et al., 1990; Remerowski et al., 1990). With the aid of the 3D experiments, we have been able to complete more proton assignments (99% of all protons as compared to 98% main-chain and 77% side-chain protons) and to identify additional remote intermolecular contacts involved in β-sheet formation. These improvements in spectral assignments provides the basis for the accurate NMR structure determination of apo-NCS.

Material and Methods

Purification of Proteins. The purifications of apo-MMC and apo-NCS were performed by reverse-phase HPLC using a Polypore polymer RP column. The proteins were eluded at 50 °C with a linear gradient (8–64% for MMC and 27–63% for NCS in 45 min) of acetonitrile/isopropanol (1:1) in 0.1% trifluoroacetic acid. The collected fractions were lyophlized to a slightly colored powder.

Protein Sequencing. Reduction and alkylation of proteins were performed by incubating the HPLC-purified material in a solution containing 6 M guanidine-HCl, 1 M Tris-HCl (pH 8.6), 10 mM EDTA, and 20 mM dithiothreitol for 1 h at 37 °C under nitrogen. 4-Vinylpyridine was then added to 50 mM and the incubation continued for 30 min at room temperature. The modified protein was desalted by HPLC according to protocols described above.

Digestion with trypsin was carried out in 0.1 M Tris-HCl (pH 8.5) for 16 h at room temperature with an enzyme to substrate ratio of 1:100. In order to recover a peptide that was lost on the subsequent separation, a second tryptic digest was carried out for 4 h at 37 °C under similar conditions. Digestion with endoproteinase Asp-N was performed with an enzyme to substrate ratio of 1:100 at room temperature for 16 h.

Peptides from the first tryptic digest and the Asp-N digest were isolated by HPLC with an Aqupore OD300 column and eluded with a linear gradient (0–64% in 90 min) of acetonitrile/isopropanol (1:1) in 0.1% trifluoroacetic acid. The second tryptic digest was isolated on a Polypore polymer RP column at 50 °C with a linear gradient of acetonitrile (0–90% in 40 min) in 0.1% trifluoroacetic acid.

Automated Edman degradations of the digests were performed with the Applied Biosystems 477A liquid-pulse sequencer. Phenylthiohydantoin amino acids were identified on an ABI 120A PTH analyzer. The complete sequences of apo-MMC and apo-NCS were obtained from the Asp-N peptides with all overlaps being confirmed by the tryptic peptides.

Two-Dimensional NMR Experiments. The NMR samples of apo-NCS and apo-MMC have concentrations of 3–4 mM and 0.8 mM, respectively, pH 4.8 ± 0.1. All NMR experiments were carried out at 30 °C with Bruker AMX600 or AMX500 spectrometers. No degradation was detected for HPLC-purified apo-NCS or apo-MMC in a several month period.

2D experiments, which include NOESY, DQF-COSY, TQF-COSY, TOCSY, DQ-COSY, and relay and double-relay COSY, in either H_2O or D_2O, were collected with 12 ppm spectral width and 1K complex data points (except for DQF-COSY, where 2K complex data points were used). Water suppression was achieved by using either presaturation or the 1–1 J–R pulse. Mixing times of NOESY experiments vary from 30, 70, 100, and 150 to 200 ms. An MLEV-17 sequence was used in TOCSY experiments with mixing times of 45, 60, 80, and 160 ms. Data processing and cross-peak volume integration were carried out by using the FELIX program (Hare Research).

Three-Dimensional NMR Experiments and Data Processing. 3D data were collected on a Bruker AMX-500 spectrometer. The 3D NOESY-TOCSY experiment (Vuister, 1988) uses a pulse sequence of [H_2O suppression–90(ϕ)–t_1–90(ϕ)–mixing–MLEV17–t_2–90–AQ(t_3)]. Pulses with time-proportional phase incrementations (TPPI) in the t_1 and t_2 dimensions are labeled by the symbol ϕ. The 3D TOCSY-NOESY experiment (Oschkinat et al., 1990) follows a pulse sequence of [H_2O suppression–90(ϕ)–t_1–MLEV17–90(ϕ)–90(ϕ)–t_2–90–AQ(t_3)]. Phase cycles for 90° pulses are as described in the literature (Vuister, 1988; Oschkinat et al., 1990) except for the MLEV17 sequence, whose phase cycle in NOESY-TOCSY is 2(x,y,–x,–y) and in TOCSY–NOESY

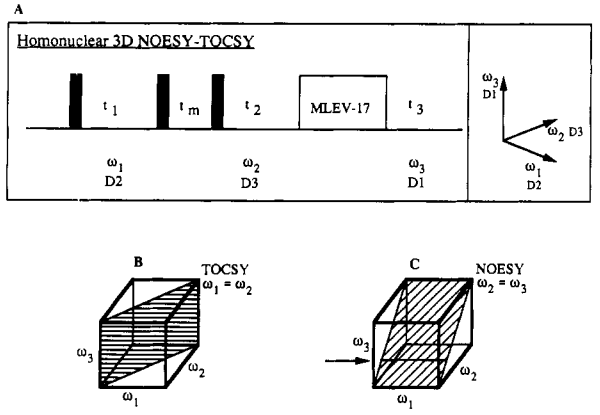

FIGURE 1: (A) Homonuclear 3D NOESY-TOCSY pulse sequence. Dimensional notations in time and frequency domains after Fourier transformation by the FELIX program (Hare Research) used in this work are indicated. (B) In a 3D NOESY-TOCSY data set, the $\omega_1 = \omega_2$ diagonal plane indicated by the shaded area is equivalent to the 2D TOCSY spectrum. This plane is useful for judging 3D data quality when compared with the corresponding 2D data. Similarly in panel C, the $\omega_3 = \omega_2$ diagonal plane indicated by the shaded area is equivalent to the 2D NOESY spectrum. The arrow points out a slice parallel to the ω_1 axis. Such slices on the diagonal planes are useful in phasing the ω_1 dimension.

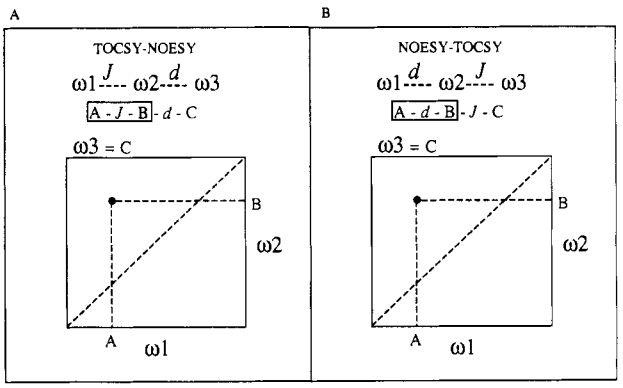

FIGURE 2: (A) TOCSY plane viewed at ω_3 = constant frequency in a 3D TOCSY-NOESY data set. The order of the spin transfer from A to B and then to C is *J*–*d*; *d* represents dipolar coupling and *J* represents scalar coupling. The *J* correlation between A and B is, thus, observed through effectively a frequency filter at the frequency of C spin by incoherent magnetization tranfer. (B) NOESY plane viewed at ω_3 = constant frequency in a 3D NOESY-TOCSY data set. The order of the spin transfer from A to B and then to C is *d*–*J*. The NOE correlation between A and B is observed through effectively a frequency filter at the frequency of C spin by coherent magnetization transfer.

is $(2x,x,-x,-x)$ with regard to the 180° pulse. Both types of experiments were run in D_2O and H_2O with HOD resonance suppressed by on-resonance preirradiation. The experimental data consist of 256 × 128 × *n* (*n* = 48–66) complex data points and were zero filled to 256 in each of the dimensions. A spectral width of 12 ppm was used. A total of 8 scans were collected for each increment with repetitive delays of 0.8–1.0 s. The NOESY mixing time was 180 ms and MLEV-17 mixing times were 20–45 ms.

3D data sets were processed by using the FELIX program (Hare Research). An unshifted skewed (skewing parameter equals 0.3) sine bell was applied to all three dimensions: D1 (ω_3), D2 (ω_1), and D3 (ω_2) (Figure 1A). Phase corrections in the second and the third dimensions can be best decided by viewing the slices on diagonal plates, such as a slice parallel to ω_1 on the $\omega_2 = \omega_3$ plane (Figure 1C). The quality of the 3D data sets can be easily examined by viewing diagonal planes, since, for a NOESY-TOCSY spectrum, the diagonal plane $\omega_1 = \omega_2$ (null NOE) is equivalent to a 2D TOCSY spectrum (Figure 1B) and the diagonal plane $\omega_2 = \omega_3$ (null *J* cross-peaks) is equivalent to a 2D NOESY spectrum (Figure 1C).

Three-Dimensional NMR Data Analysis. In a TOCSY-NOESY spectrum, the axes defining the TOCSY planes are ω_1 and ω_2 and the axes defining the NOESY planes are ω_2 and ω_3, respectively. By analogy, ω_1 and ω_2 in a NOESY-TOCSY spectrum defines the NOESY plane and ω_2 and ω_3 the TOCSY planes, respectively. In our experience, the appearance of the ω_1/ω_2 plane in a 3D NMR experiment is always cleaner than that of the ω_2/ω_3 plane. This is to say that better TOCSY planes were obtained from the TOCSY-NOESY experiment and better NOESY planes were obtained from the NOESY-TOCSY experiment.

Each off-diagonal cross-peak represented by ω_1, ω_2, and ω_3 in a 3D data set correlates the interactions between three spins. The interpretation of these correlations depends on the type of the experiment. A cross-peak in a TOCSY-NOESY spectrum represents spin A resonating at ω_1 scalar coupled to spin B at ω_2 and spin B dipolar coupled to spin C at ω_3. This relationship can be simply expressed as $A(\omega_1)$–*J*–$B(\omega_2)$–*d*–$C(\omega_3)$ (the dipolar correlation is designated by *d*, and the through bond correlation is designated by *J*). Likewise, a cross-peak in the NOESY-TOCSY experiment reveals the correlations of $A(\omega_1)$–*d*–$B(\omega_2)$–*J*–$C(\omega_3)$. Comparing to 2D data sets, the planes in a 3D spectrum are simplified by effectively filtering through a frequency filter as shown in Figure 2A and 2B.

The use of the 3D data to resolve ambiguous assignments is illustrated in Figure 3, which illustrate two sets of spins consisting of A1, B1, C1, and C2 as well as A2, B2, C3, and C4 with the chemical shifts of spins B1 and B2 indistinguishable (note that the A spins may not be necessarily *J*-coupled to the B spins). In this case, 2D data can not provide definitive assignments (Figure 3A and 3B). In a 3D spectrum, such overlaps can be identified by correlating to the difference in the frequencies of spins A1 and A2 (Figure 3C). Examples of applying 3D NMR data in apo-NCS proton assignments will be detailed under Results and Discussion.

Results and Discussion

The Sequences of Apo-NCS and Apo-MMC

MMC isolated from *Streptomyces malayensis* is known to be a member of the same antitumor protein family as NCS isolated from *Streptomyces carzinostaticus*. Little information was available about the structure of apo-MMC and its non-protein component. Although sequencing the first 37 residues and preliminary crystallization studies indicated the similarity between apo-MMC and apo-NCS, the conclusion was obscured by the observed inconsistency in the amino acid composition analysis of apo-MMC to that of apo-NCS (Sieker & Gnanarajah, 1988). We carried out amino acid analysis and completely sequenced HPLC-purified apo-MMC along with apo-NCS for comparison by automated Edman sequencing method. Our results conclusively show that the primary sequence of apo-MMC is identical with that of apo-NCS as shown in Scheme I. The comparison of the NOESY spectra of apo-MMC and apo-NCS is given in Figure S1 (supplementary material). Proton chemical shifts are identical for both proteins as judged from NOESY (Figure S1) and COSY (unpublished data) cross-peak positions, supporting the conclusion based on sequencing and composition analysis.

We found two records of apo-NCS sequence from a protein data base search (Gilson et al., 1984; Kuromizu et al., 1986).

Scheme I

Apo-Neocarzinostatin

1 10 20
Ala - Ala - Pro - Thr - Ala - Thr - Val - Thr - Pro - Ser - Ser - Gly - Leu - Ser - Asp - Gly - Thr - Val - Val - Lys - Val - Ala - Gly - Ala - Gly -
30 40 50
Leu - Gln - Ala - Gly - Thr - Ala - Tyr - Asp - Val - Gly - Gln - Cys - Ala - Trp - Val - Asp - Thr - Gly - Val - Leu - Ala - Cys - Asn - Pro - Ala -
60 70
Asp - Phe - Ser - Ser - Val - Thr - Ala - Asp - Ala - Asn - Gly - Ser - Ala - Ser - Thr - Ser - Leu - Thr - Val - Arg - Arg - Ser - Phe - Glu - Gly -
80 90 100
Phe - Leu - Phe - Asp - Gly - Thr - Arg - Trp - Gly - Thr - Val - Asp - Cys - Thr - Thr - Ala - Ala - Cys - Gln - Val - Gly - Leu - Ser - Asp - Ala -
110 113
Ala - Gly - Asn - Gly - Pro - Glu - Gly - Val - Ala - Ile - Ser - Phe - Asn

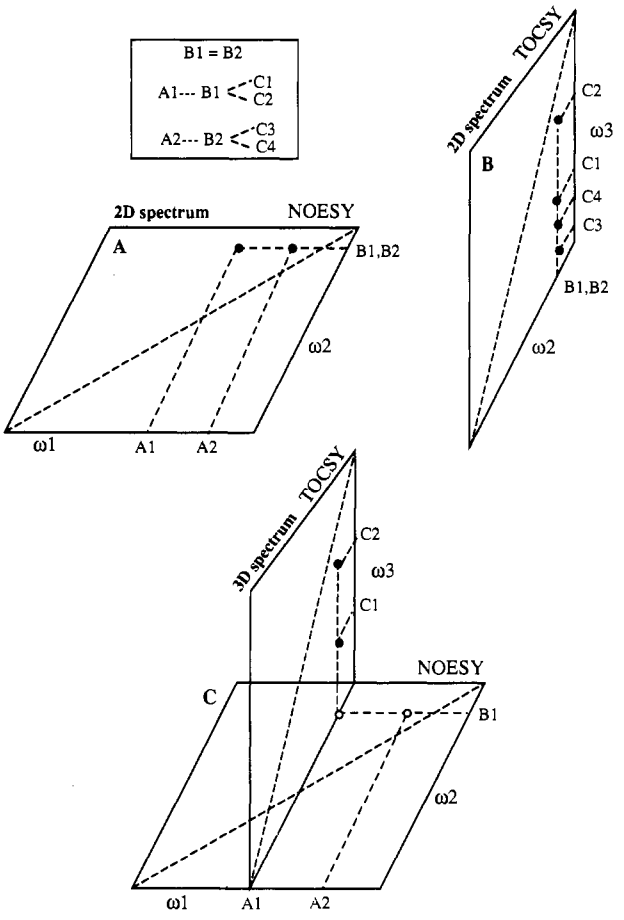

FIGURE 3: Illustration of the use of 3D data to resolve overlapped 2D cross-peaks in two groups of spin systems. (A) Pictorial 2D NOESY spectrum containing two cross-peaks for A1/B1 and A2/B2; A and B spins can be either J or NOE correlated. (B) Pictorial 2D TOCSY spectrum containing the correlations between several B and C spins. This 2D spectrum does not provide definitive spin-system assignments due to the overlap of B1 and B2 resonances. (C) 3D data display. In a 3D data set, the ambiguity in (B) can be resolved by examining planes viewed through the frequency of a third spin. The TOCSY plane indicates that A1 is only related to C1 and C2 and likewise A2/(C3 and C4) correlation can be determined from the TOCSY plane at the A2 frequency (plane not shown).

The primary sequence assignments in these two sequences are different in positions of 41, 48, 51, and 103 (Table I). Our sequence determination of apo-MMC and apo-NCS establishes residues 41 and 51 as Asp and 48, 60, and 103 as Asn (Table I), respectively. This result is different from that of the latest sequencing of apo-NCS in position 60 (Kuromizu et al., 1986). As reported by recent NMR studies (Adjadj et al., 1990; Lyndsay et al., 1990), we also observed the terminal amide protons at 7.70 and 6.81 ppm for residue 60, confirming that residue 60 should be an Asn. However, we can not detect the terminal amide protons at position 48, possibly due to their fast exchange with solvent. Since natural MMC and NCS have been reported as possessing different biological profiles (Montgomery et al., 1981), it would be interesting to find whether the nonprotein components of MMC and NCS are identical.

Table I: Asn and Asp Assignments from this Work and Existing Literature for the Apo-NCS Sequence[a]

	residue				
	41	48	51	60	103
this work	D	N	D	N	N
pub I[b]	*N*	*D*	*N*	*D*	*D*
pub II[c]	D	N	D	*D*	N
NMR[d]	D	*D*	D	N	N

[a] Only those with discrepancy are listed. [b] Gilson et al. (1984), residues different from our result are in italic. [c] Kuromizu et al. (1986). [d] Remerowski et al. (1990).

Since apo-MMC and apo-NCS are in fact the same molecule, the following discussion refers to apo-NCS only.

Spin-System Identification

In order to adopt a semiautomated cross-peak assignment procedure, which is described later, our initial effort focused on spin-system identifications (Wüthrich, 1986). For apo-NCS of 113 amino acid residues, most of the 2D COSY spectrum is still reasonably well resolved. We were able to identify over 95% of the spin systems by using combined 2D and 3D analyses prior to the sequential assignments. The majority of the proton assignments were published as this work was in progress (Adjadj et al., 1990; Remerowski et al., 1990). Here, we present and discuss the discrepancies in assignments, the new assignments, and the application of 3D NMR data in spin-system identifications.

Ala Residues. Figure 4 shows an expanded TOCSY spectrum correlating amide protons with Hα and Hβ protons. A total of 15 Ala HN/Hα coupling cross-peaks out of the 18 Ala residues in apo-NCS appeared in this region. Our assignments for the Ala spin systems in general agree with published data except for two Ala residues [Figure 4, Ala(2) underlined], which were later determined as terminal Ala(1) and Ala(2), respectively. We found that the assignments for the Hα and Hβ resonances of Ala(1) and Ala(2) residues should be interchanged for those reported earlier (Adjadj et al., 1990; Table S1, supplementary material). Our assignments of the Ala(1) and Ala(2) spin systems were later confirmed as a strong interaction was detected between the Hα of Ala(2) [which would be Hα of Ala(1) according to Adjadj et al. (1990)] and the Hα of Pro(3).

Gly Residues. Figure S2 (supplementary material) gives expanded DQ-COSY (top) and DQF-COSY (bottom) spectra. The DQ-COSY plot contains *J* cross-peaks of the remote connectivities between the HN and Hα protons of Gly residues, and the DQF-COSY plot contains cross-peaks of coupled HN and Hα protons. A total of 13 out of the 15 Gly residues can be identified by their distinct coupling cross-peak patterns in the DQF-COSY spectrum (cross-peaks linked by solid lines in Figure S2, supplementary material). The identification of the last two Gly residues was aided by the remote connectivity cross-peaks in DQ-COSY spectrum as indicated in Figure S2

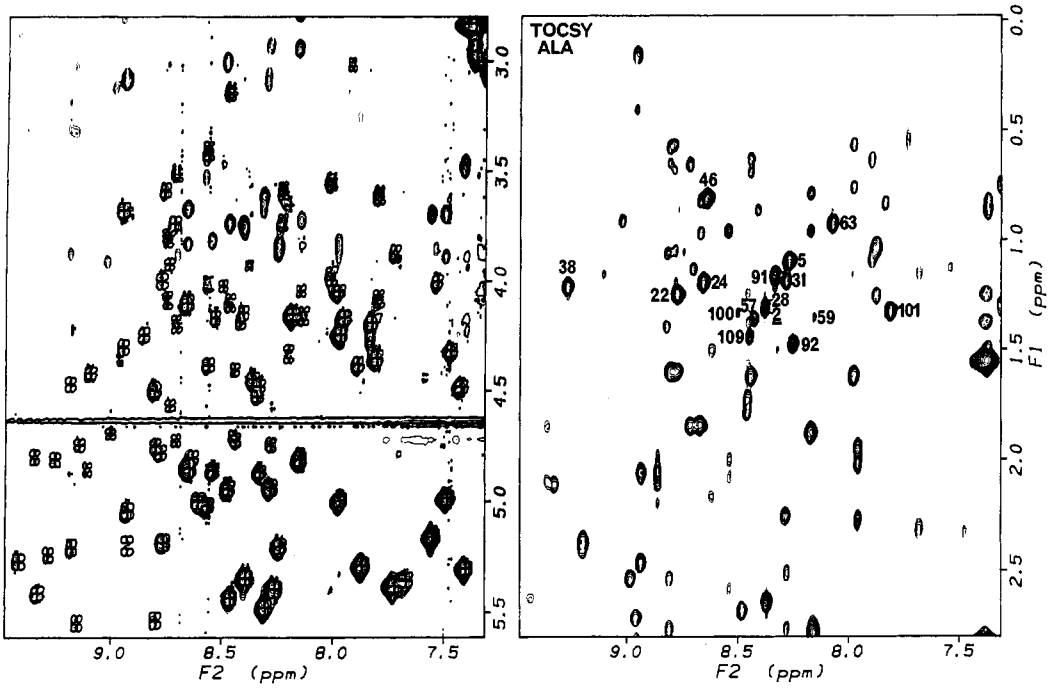

FIGURE 4: Fingerprint region connecting HN/Hα (spectrum on left) and HN/Hβ (spectrum on right) protons in 2D DQF-COSY (spectrum on left only) and TOCSY (45-ms mixing time) spectra recorded in H_2O (all spectra shown are referred to apo-NCS unless noted). Most J cross-peaks are well resolved. The relayed HN/Hβ correlation of the Ala residues are labeled (spectrum on the right). The Ala(2) Hβ (underlined residue in the spectrum on the right) was assigned to Ala(1) Hβ (Adjadj et al., 1990).

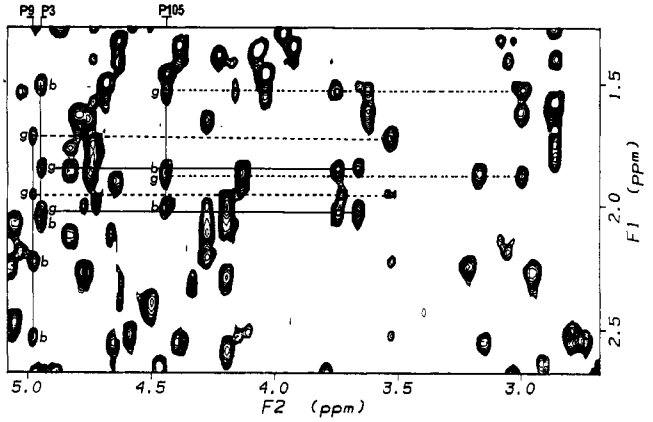

FIGURE 5: Explanded plot of the 2D TOCSY spectrum recorded in D_2O. This plot gives correlations (vertical solid lines) between the Hα (F_2 axis) and Hβ and Hγ (F_1 axis) protons for three out of the four Pro residues. The positions of the Hα resonances are indicated on top of the plot. The cross-peaks connecting the Hγ (on F_1 axis) with Hδ (on F_2 axis) protons in relevant Pro residues are indicated by open circles on horizontal lines.

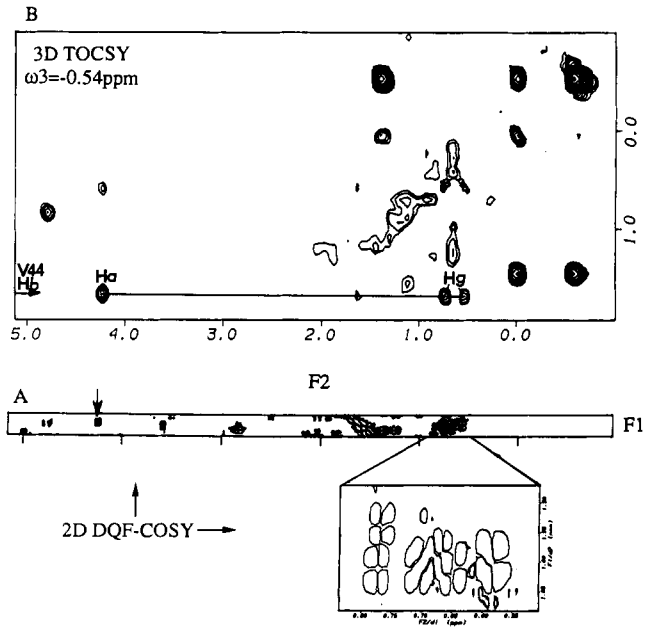

FIGURE 6: Use of combined 2D and 3D data analysis for assigning Val spin systems. (A) Expanded 2D DQF-COSY spectrum in the region of Hα, Hβ, and Hγ (F_2 axis)/Hβ (F_1 axis). The overlapped Hγ/Hβ cross-peak region for Val residues is further expanded. Peak indicated by an arrow is a Val Hα/Hβ cross-peak. The spin system Hα–Hβ–Hγ related to this peak can not be determined from the 2D spectrum. (B) TOCSY plane at –0.54 ppm in a 3D TOCSY-NOESY spectrum recorded in H_2O. The Val spin system can be unambiguously identified through intraresidue coupling cross-peaks Hα/Hβ (labeled as Hα) and Hγ/Hβ (labeled as Hγ). Other overlapped 2D cross-peaks have been filtered out.

(supplementary material). The chemical shifts of the Hα resonances of Gly(104), which were not reported in earlier studies (Adjadj et al., 1990), were estimated from the DQ-COSY data by assuming one of the Hα resonances close to that of HOD according to the relationship of $\omega_1 = \omega(H\alpha 1) + \omega(H\alpha 2)$ (Wüthrich, 1986).

Pro Residues. The assignments of the Pro resonances were achieved by carefully analyzing the TOCSY spectrum recorded in D_2O after the majority of the COSY cross-peaks had been identified. Three out of the four Pro spin systems can be traced by the relay coupling correlations between the Hα and Hγ protons as shown in Figure 5. The assignments of the Hα and Hβ resonances of the fourth Pro residue were made during the semiautomated NOE cross-peak analyses through their interaction with the protons of adjacent residues. The published NMR results have only few proline protons assigned and some of these assignments do not agree with ours (Table S1, supplementary material).

Val, Leu, and Ile Residues. The spin-system identification of the Val and Ile residues presented some difficulty due to severe overlaps of the methyl proton resonances as shown in Figure 6A, which consequently render ambiguities in identifying the Hβ and Hγ correlations. In these cases, 3D data

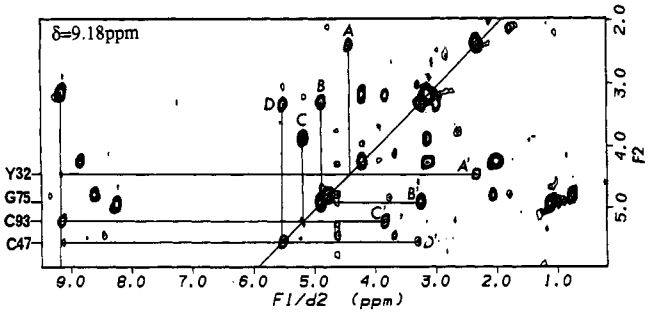

FIGURE 7: TOCSY plane at 9.18 ppm in a 3D TOCSY-NOESY spectrum. This plane contains scalar connectivities (horizontal lines) of HN_i-*d*-$\underline{H\alpha_i}$-*J*-$\underline{H\beta_i}$ and HN_i-*d*-$\underline{H\beta_i}$-*J*-$\underline{H\alpha_i}$ for residues 32, 47, 75, and 93 with observed correlations underlined. The Hα protons resonate at 4.3–5.8 ppm (indicated on the left of the plot) and the Hβ protons resonate at 2.0–4.0 ppm. Peak A', HN_{32}-*d*-$\underline{H\alpha_{32}}$-*J*-$\underline{H\beta_{32}}$; peak B', HN_{75}-*d*-$\underline{H\alpha_{75}}$-*J*-$\underline{H\beta_{75}}$; peak C', HN_{93}-*d*-$\underline{H\alpha_{93}}$-*J*-$\underline{H\beta_{93}}$; peak D', HN_{47}-*d*-$\underline{H\alpha_{47}}$-*J*-$\underline{H\beta_{47}}$; peak A, HN_{32}-*d*-$\underline{H\beta_{32}}$-*J*-$\underline{H\alpha_{32}}$; peak B, HN_{75}-*d*-$\underline{H\beta_{75}}$-*J*-$\underline{H\alpha_{75}}$; peak C, HN_{93}-*d*-$\underline{H\beta_{93}}$-*J*-$\underline{H\alpha_{93}}$; peak D, HN_{47}-*d*-$\underline{H\beta_{47}}$-J-$\underline{H\alpha_{47}}$.

were found to be useful. For instance, as shown in Figure 6A, it would have been impossible to identify the correlation of the indicated peak to its own methyl. However, in the TOCSY plane (ω_3 = –0.54 ppm) of the TOCSY-NOESY spectrum (Figure 6B), the connectivities of Hα–Hβ–Hγ protons of the Val residue can be easily identified through the scalar correlations of Hα and Hγ protons with Hβ proton. Other overlapped 2D cross-peaks do not appear on this plane (Figure 6B). By using combined 2D and 3D data analyses, we have assigned all of the proton resonances of Val and Ile residues. Minor disagreement with recent NMR studies was found for some of the Ile resonance assignments (Table S1, supplementary material).

General Applications of 3D Data. 3D spectra can be viewed through the TOCSY or the NOESY planes (for the plane definitions, see the paragraph concerning 3D NMR data analysis under Material and Methods). The TOCSY planes are more suitable for spin-system analysis, since the coupling cross-peaks can be directly observed and compared with those in 2D TOCSY spectra. As an example, the expanded TOCSY plane of the TOCSY-NOESY data set viewed at the HN frequency (9.18 ppm) of the residues 32, 47, 75, and 93 is given in Figure 7. This plane contains *J* coupling cross-peaks related to the HNs resonating at 9.18 ppm, that is, HN_i-*d*-$\underline{H\alpha_i}$-*J*-$\underline{H\beta_i}$ and HN_i-*d*-$\underline{H\beta_i}$-*J*-$\underline{H\alpha_i}$ (observed *J* correlations in the TOCSY plane are underlined). For instance, cross-peak A in Figure 7 corresponds to the coupling connectivity between the Hβ (2.38 and 2.40 ppm on the F_2 axis) and Hα (4.47 ppm on the F_1 axis) protons of tyrosine 32. This cross-peak was observed because of the NOE connectivity between the Hβ and the HN (9.18 ppm) protons in residue 32, given by HN_{32}-*d*-$\underline{H\beta_{32}}$-*J*-$\underline{H\alpha_{32}}$. Cross-peak A' reflects the coupling correlations between the Hα (4.47 ppm on the F_2 axis) and Hβ (2.38 and 2.40 ppm on the F_1 axis) protons through the NOE correlation between the Hα and HN (9.18 ppm) protons, given by HN_{32}-*d*-$\underline{H\alpha_{32}}$-*J*-$\underline{H\beta_{32}}$. The Hα resonances of residues 47, 75, and 93 are also indicated in Figure 7 on the F_2 axis. Each of these Hα protons exhibits 3D coupling cross-peaks following similar relationships described above. Fixed frequencies on the third axis can also be chosen at the Hα region; the correlations observed on the TOCSY planes, in this case, are between the HN and Hβ and between the HN and Hγ resonances.

3D TOCSY analyses helped to identify one of the three Arg residues, whose spin connectivities can not be unambiguously determined from 2D data. Two out of the three Arg spin systems were easily identified by starting from the strong coupling cross-peaks between the Hδ and the terminal ammonium protons. However, the connectivities of the third Arg were broken at the β–γ step. This missing link was connected by examining the TOCSY plane at the HN frequency of the third Arg residue. Subsequently we were able to identify the cross-peaks correlating the HN with the Hβ and Hγ (data not shown). The chemical shifts of Arg residues and disagreement with reported assignments are listed in Table S1 (supplementary material). At present, the efficient utilization of 3D data is partly limited by the unavailability of the general data management programs, although numbers of such programs are emerging. It is expected that once such programs are readily available, 3D NMR spectra will find wide applications in spin-system identifications of macromolecules, especially in cases where 2D would fail to provide definitive assignments.

Semiautomated NOE Cross-Peak Assignments

The complexity of the NOESY spectra of apo-NCS were evident from ~2230 major cross-peaks at 200-ms mixing time and ~1200 major cross-peaks at 70-ms mixing time. This made us realize that we have to modify the conventional strategies for proton resonance assignment to deal with spectra of this complexity.

General Strategy. We chose first to generate two files: the cross-peak file, which contains the coordinates (in unit of data point or ppm) and the volume of each cross-peak, and the spin assignment file, which contains the names of the identified spins and their chemical shifts or coordinates (in unit of data point or ppm). The spin identifications were tentative at first and revised as resonance assignments proceeded. From these two files, all of the possible spin–spin interactions for each of the NOE cross-peaks in the NOESY spectra with different mixing times were listed. There are about 6000 spin–spin interactions listed for the NOESY spectrum obtained at 70-ms mixing time, an average 5 possible interactions per cross-peak. By doing so, it is less likely to omit NOE assignments arising from unexpected proton–proton contacts. One practical problem is that the alignment of the coordinates in cross-peak files and in the spin identification file requires a perfect match. However, the positions of a cross-peak in various spectra collected at different times and solvent conditions (H_2O vs D_2O) are not always identical due to slight temperature and pH shifts. It would be very tedious to do systematic corrections for each data set, and in some cases corrections can not even be made by systematic corrections. To overcome this problem, we constructed a reference cross-peak file whose coordinate scale is consistent with that in the spin identification file. This reference file was edited such that it can be used as a template to match all the cross-peaks in 2D and 3D (with proper conversions due to lower digital resolution used in 3D experiments) data sets. For instance, peak 1 in the reference file has the coordinates 9.25 and 5.00 ppm. This set of coordinates will be used to represent the same cross-peak in different spectra, such as NOESY at different mixing times and DQF-COSY, no matter that this cross-peak is at 9.26 and 5.01 ppm (systematic shift) in the NOESY spectrum (30-ms mixing time) and 9.24 and 5.02 ppm (nonsystematic shift) in the DQF-COSY spectrum. In other words, this is to assign each cross-peak a set of pseudocoordinates. The match between the cross-peaks in the reference file and those in the experimental spectrum can be easily decided by pattern recognition with the FELIX program (Hare Research).

The next step then was the assignments of proton resonances

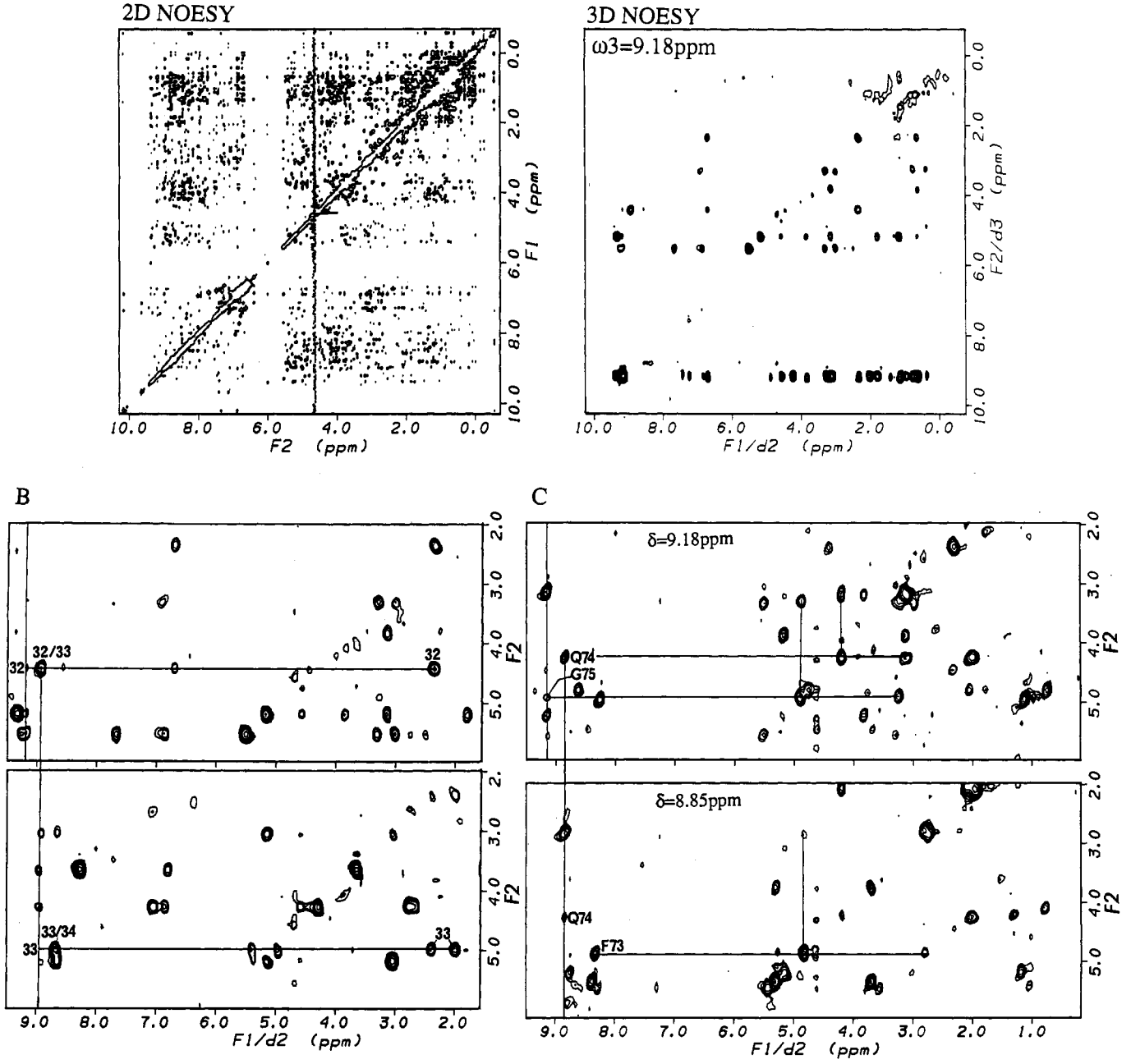

FIGURE 8: (A) Full 2D NOESY plot (200-ms mixing time) on the left and NOESY plane at 9.18 ppm in a 3D NOESY-TOCSY spectrum (180-ms mixing time) on the right. Both data sets were recorded in H_2O. (B) Illustration of sequential connectivities from i to $i+1$ and to $i+2$ residues by expanded NOESY planes at 9.18 ppm (top) and 8.92 ppm (bottom) in a 3D NOESY-TOCSY spectrum. The top plot shows distance connectivities of $H\alpha_{32}$ (F_2, 4.47 ppm)/$H\beta_{32}$ (F_1, 2.38, 2.40 ppm) and $H\alpha_{32}$ (F_2, 4.47 ppm)/HN_{33} (F_1, 8.92 ppm) through the J correlation of HN_{32} (9.18 ppm)/$H\alpha_{32}$. The bottom plot shows distances connectivities of $H\alpha_{33}$ (F_2, 5.04 ppm)/$H\beta_{33}$ (F_1, 2.06, 2.46 ppm) and $H\alpha_{33}$ (F_2, 5.04 ppm)/HN_{34} (F_1, 8.70 ppm) through the J correlation of HN_{33} (8.92 ppm)/$H\alpha_{33}$. (C) Illustration of sequential connectivities from i to $i-1$ and to $i-2$ residues by expanded TOCSY planes at 9.18 ppm (top) and 8.85 ppm (bottom) in a 3D TOCSY-NOESY spectrum. The top plot shows J connectivities of $H\alpha 1_{75}$ (F_2, 4.89 ppm)/$H\alpha 2_{75}$ (F_1, 3.30 ppm) and $H\alpha_{74}$ (F_2, 4.24 ppm)/HN_{74} (F_1, 8.85 ppm) through the d correlations of HN_{75} (9.18 ppm)/$H\alpha 1_{75}$ and $HN_{75}/H\alpha_{74}$, respectively. The bottom plot shows the J connectivities of $H\alpha_{73}$ (F_2, 4.86 ppm)/HN_{73} (F_1, 8.32 ppm) through the d correlation of HN_{74} (8.85 ppm)/$H\alpha_{73}$.

and NOE cross-peaks on the basis of the list of spin–spin interactions described above.

Main-Chain Sequential Connectivities. The initial proton assignments were focused on sequential connectivities of HN and Hα (for some residues also Hβ) protons by examining the spin–spin interaction list based on established rules (Wüthrich, 1986). This result is listed in Table S1 (supplementary material) and agrees in general with those reported recently (Adjadj et al., 1990; Remerwoski et al., 1990). One major difference is that the HN proton resonance of Thr(4) should be assigned to 8.87 (0.14 ppm was added as a correction factor) instead of 8.45 ppm (Adjadj et al., 1990) as determined by both COSY and NOESY experiments. There are 10 resonances resonating at frequencies very close to that of HOD and that can only be observed in NOESY experiments using the jump–return reading pulse as shown in Figure S3 (supplementary material).

Figure 8A illustrates the contrast in complexity of a 2D NOESY spectrum and a NOESY plane in a 3D data set. The simplification in cross-peak overlaps by 3D data is helpful in

the complete and unambiguous assignments of NOE cross-peaks. Especially useful are the NOESY planes at the frequency region of HN resonances, which contain the intraresidue NOEs ($H\alpha_i/HN_i$ and $H\alpha_i/H\beta_i$, etc.) and the interresidue NOEs ($H\alpha_i/HN_{i+1}$, note the direction is i to $i+1$) through a J filter at the frequency of HN_i (Figure 8B). The sequential connectivities are then found from the next NOESY plane at the frequency of HN_{i+1} and so on. Figure 8B demonstrates that the NOE connectivities from residue 32 to 33 to 34 can be unambiguously determined with the assistance of 3D data, even though the HN of Asp(33) has a chemical shift almost identical with those of Gly(23) and Asp(99) (Table S1, supplementary material). The sequential connectivities in the TOCSY planes are less transparent, as shown in Figure 8C. Such a plane contains coupling cross-peaks within the i and $i-1$ residues (note the direction is i to $i-1$) through an NOE filter at the frequency of HN_i (Figure 8C). Since the coupling cross-peaks of the $i-1$ residues can be anywhere in the TOCSY plane, the spectrum is less informative for tracing the connectivity of a cross-peak to its adjacent residues (Figure 8C). However, the TOCSY plane is still useful in confirming assignments from 2D data, in this case only the existence of a cross-peak needs to be identified. It is interesting to notice that the tracing direction of the sequential connectivities in the NOESY planes follow the direction of i to $i+1$ and $i+1$ to $i+2$, etc., and is opposite to that in the TOCSY plane, which follows i to $i-1$ and $i-1$ to $i-2$, etc.

3D Analyses of Remote Connectivities. The spin–spin interaction list reveals a large number of proton–proton contacts between remote residues. When there exist extensive overlaps, it is rather difficult to differentiate the real from false ones. Figure 9 shows two such examples. Figure 9A is an expanded plot of the NOESY plane at the frequency of HN_{47} and shows that the Hα proton (5.54 ppm) of Cys(47) exhibits an NOE to its own Hβ protons (3.03 and 3.33 ppm) and to the Hβ protons (2.54 and 2.77 ppm) of Cys(37) as well. These remote interactions between Cys(47) and Cys(37) residues can not be assigned from the 2D spectra, since the chemical shifts of the Hα protons of these two residues are identical (Table S1, supplementary material). The second example concerns peak 226 (as numbered in the cross-peak file), which was listed possibly correlating at least two sets of interactions: between the Hα protons of residues 48 and 22 (5.35 and 5.18 ppm) and/or between the Hα protons of residues 64 and 22 (5.35 and 5.18 ppm). Figure 9B,C illustrates how this ambiguity can be resolved by examining the NOESY planes at the frequencies of HN protons of residues 64 at 8.46 ppm (Figure 9B) and 48 at 7.67 ppm (Figure 9C), respectively. A strong NOE cross-peak at 5.35/5.18 ppm was detected in Figure 9B, indicating the close contact between the Hα protons of residues 64 and 22. In contrast, the same cross-peak is absent in Figure 9C.

By carefully analyzing 2D and 3D data, we have assigned about 1270 NOEs (NOEs from hydrogen atoms of fixed distances are not included) accounting for intra- and interresidue (sequential and remote) proton–proton interactions. These assignments permitted the generation of the initial structures by restrained molecular dynamics with the XPLOR program (unpublished results). Further structure refinement should furnish the complete assignment of all NOE cross-peaks.

Methods for Analyzing Overlapped HN/Hα Cross-Peaks

The emphasis of the 3D application in this work is to develop methods useful for assigning overlapped 2D NOE cross-peaks.

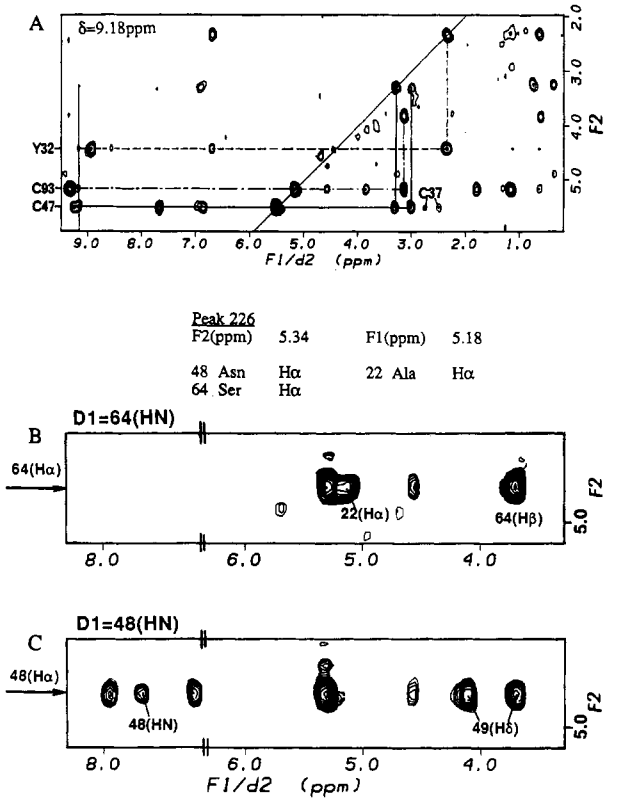

FIGURE 9: (A) Expanded NOESY plane at 9.18 ppm in a 3D NOESY-TOCSY spectrum. In this plot, two cross-peaks (labeled C37) are due to remote distance connectivities linking to Cys(47) Hα (F_2, 5.53 ppm) and Cys(37) Hβ (F_1, 2.54, 2.76 ppm) protons. 2D data can not provide this information, since the Hα protons of residues 37 and 47 are identical (Table S1, supplementary material). (B) Expanded NOESY plane at HN_{64} frequency in a 3D NOESY-TOCSY spectrum. This plot contains a strong NOE cross-peak consistent with $H\alpha_{64}$ (F_2, 5.33 ppm)/$H\alpha_{22}$ (F_1, 5.18 ppm), providing the unambiguous assignment for peak 226. (C) Expanded NOESY plane at HN_{48} frequency in a 3D NOESY-TOCSY spectrum. The $H\alpha_{48}$ (F_2, 5.33 ppm)/$H\alpha_{22}$ (F_1, 5.18 ppm) NOE cross-peak is absent.

For apo-NCS, there are three types of overlapped NOE cross-peaks in the fingerprint region of the 2D spectra. These three types of overlapped cross-peaks can be resolved by the different approaches described below.

Type I: Superimposed 2D Cross-Peaks from the Same Residue. This category of cross-peaks shown in Table II in bold lettering arise from covalently linked protons (linkage designated by J). Extended correlations on the third dimension for a particular cross-peak are also listed, illustrating the possibility for identifying these type of overlaps *by chemical shift differentiation of the third spins in the third dimension.* For instance, the overlap between residues 31 and 39 can be identified by examining the TOCSY planes at the Hα frequencies of residues 30 and 38 or at the HN frequencies of residues 32 and 40 (Table II, entry 1), as the Hα resonances of residues 30 and 38 and the HN resonances of 32 and 40 are well resolved (Table S1, supplementary material). As a practical choice, using HN proton frequencies as the third dimension is preferred due to their larger chemical shift dispersion and separation from the water signal. It is noted that 3D cross-peaks may not always be observed as predicted (Table II, part of entry 1 and 2), since the intensities of observed cross-peaks are products of two-step magnetization transfer. Nonetheless, in principle, type I superimposed cross-peaks should be resolvable by examining the TOCSY planes at the frequencies of the third spins connected to the overlapped cross-peak on the third dimension.

Table II: Type I Superimposed 2D Cross-Peaks[a]

	connectivities of overlapped cross-peaks	observed 3D connectivity
1	30(Hα)–^{d}–**31(HN)**–^{J,d}–**31(Hα)**–^{d}–32(HN)	**31(HN)–31(Hα)**–32(HN)
	38(Hα)–^{d}–**39(HN)**–^{J,d}–**39(Hα)**–^{d}–40(HN)	**39(HN)–39(Hα)**–40(HN)
2	23(Hα)–^{d}–**24(HN)**–^{J,d}–**24(Hα)**–^{d}–25(HN)	23(Hα)–**24(HN)–24(Hα)**
	52(Hα)–^{d}–**53(HN)**–^{J,d}–**53(Hα)**–^{d}–54(NH)	52(Hα)–**53(HN)–53(Hα)**
3	5(Hα)–^{d}–**6(HN)**–^{J,d}–**6(Hα)**–^{d}–7(HN)	5(Hα)–**6(HN)–6(Hα)**
	57(Hα)–^{d}–**58(HN)**–^{J,d}–**58(Hα)**–^{d}–59(HN)	57(Hα)–**58(HN)–58(Hα)** **6(HN)–6(Hα)**–7(HN) **58(HN)–58(Hα)**–59(HN)

[a] *d*, through distance correlations; *J*, through bond correlations. Spin pairs in bold lettering indicate overlapped intraresidue 2D cross-peaks.

Table III: Type II Superimposed 2D Cross-Peaks[a]

	connectivities of overlapped cross-peaks	observed 3D connectivity
1	22(HN)–^{J}–**22(Hα)**–^{d}–**23(HN)**	22(HN)–22(Hα) on TOCSY plane
	23(HN)–^{J,d}–**23(Hα)**–^{d}–24(HN)	23(Hα)–24(HN) on NOESY plane
2	41(Hα)–^{d}–**42(HN)**–^{J,d}–**42(Hα)**	
	42(Hα)–^{d}–**43(HN)**–^{J}–43(Hα)	43(HN)–43(Hα) on TOCSY plane
3	58(Hα)–^{d}–**59(HN)**–^{J,d}–**59(Hα)**	59(HN)–59(Hα) on TOCSY plane[b]
	59(Hα)–^{d}–**60(HN)**–^{J}–60(Hα)	
4	91(HN)–^{J}–**91(Hα)**–^{d}–**92(HN)**	91(HN)–91(Hα) on TOCSY plane
	92(HN)–^{J,d}–**92(Hα)**–^{d}–93(HN)	92(Hα)–93(HN) on NOESY plane

[a] *d*, through distance correlations; *J*, through bond correlations. Spin pairs in bold lettering indicate sequential and intraresidue 2D cross-peaks from adjacent residues. [b] Observed at the frequencies of Hβ protons of residue 58.

Type II: *Superimposed 2D Cross-Peaks from Adjacent Residues*. Overlaps also occur due to the degeneracy of the HN resonances (Table III, entries 1 and 4) or the Hα resonances (Table III, entries 2 and 3) from consecutive residues. The overlaps of this type can be identified by *the uniqueness of the order of spin transfer reflected in 3D spectra*. For instance, in Table III, entry 4, the order of the magnetization transfer from spins 92 (HN) to 91 (Hα) and then to 91 (HN) can be expressed as *d*–*J*, and that from spins 92(HN) to 92(Hα) and then to 93(HN) is *J*–*d* [note that both spin connectivity sequence starting with 92 (HN)]. Under these circumstances, 2D data can not provide independent NOE assignments for 91 (Hα)/92 (HN) and 92 (Hα)/92 (HN). However, in a 3D data set, the TOCSY plane at the frequency of 92 (HN) gives only the *J*-correlated cross-peak (HN/Hα) of residue 91, and a NOESY plane at the same HN frequency gives only the NOE cross-peak [92 (Hα)/93 (HN)], providing unambiguous assignment for two sets of spin connectivities related to 92 (HN) resonance in an indirect way as given in Table III (entry 4).

Type III: *Superimposed 2D Cross-Peaks from Unrelated Residues*. These are overlapped scalar-coupled or distance-related cross-peaks from protons of unrelated residues (Table IV). The ambiguities arise since sequential NOEs, such as 63 (Hα)/64 (HN), are located under those of covalently bound protons, such as 2 (HN)/2 (Hα) (Table IV, entry 1). Both methods discussed above, that is, the chemical shift differentiation in the third dimension (for type I overlapped cross-peaks) or the spin transfer order differentiation (for type II overlapped cross-peaks), can be applied as shown in Table IV. For similar reasons discussed above, some of the predicted 3D cross-peaks were not observed (Table IV). Possible solutions may be found in multiple data sets with different combinations of spin lock and NOE mixing times.

Table IV. Type III Superimposed 2D Cross-Peaks[a]

	connectivities of overlapped cross-peaks	observed 3D connectivity
1	1(Hα)–^{d}–**2(HN)**–^{J,d}–**2(Hα)**–Pro	
	63(HN)–^{J}–**63(Hα)**–^{d}–**64(HN)**–^{J}–64(Hα)	**63(Hβ)–64(HN)**–64(Hα)
2	40(Hα)–^{d}–**41(HN)**–^{J,d}–**41(Hα)**–^{J}–42(HN)	
	4(HN)–^{J}–4(Hα)–^{d}–**5(HN)**–^{J}–5(Hα)	**4(Hβ)–5(HN)**–5(Hα)

[a] *d*, through distance correlations; *J*, through bond correlations. Spin pairs in bold lettering indicate overlapped intraresidue and sequential 2D cross-peaks from remote residues.

Secondary Structure of Apo-NCS

The sequential connectivities of apo-NCS are summarized in Table S2 (supplementary material) and are in agreement with those by recent 2D NMR studies (Adjadj et al., 1990; Remerowski et al., 1990). Several turns in apo-NCS sequence responsible for the secondary folding are well defined by the disruption in NOE patterns characteristic of β-sheet structure (Table S2) (Wüthrich, 1986). In addition to previously reported six β-sheet motif (Remerowski et al., 1990), we also found interactions between the amide protons of residues 8 and 20, between the amide and Hα protons of residues 5 and 23, and between the Hα protons of residues 5 and 23 as well as residues 3 and 25. This result allows the antiparallel alignment of the segments from residues 3 to 8 and from residues 20 to 25 (Figure S4, supplementary material), providing the seventh β-sheet in apo-NCS. The relative alignments of all seven β-sheets are drawn in Figure S5 (supplementary material).

Figure S6 (supplementary material) shows an overlay NOESY plot (samples differ in pH by ~0.4 unit) covering HN/Hα and HN/Hβ region. While most cross-peaks are well superimposed, several resonances exhibited a noticeable shift relative to each other. These shifted resonances are the HN protons from residues 99, 100, 101, 102, and 103 (Figure S6, supplementary material), indicating that this loop region (Table S2 and S5, supplementary material) is highly solvent

accessible. It is interesting that this segment is within the proposed binding sequence in holo-NCS.

Conclusions

The strategy of the semiautomated NOE cross-peak assignment relies on the construction of a reference cross-peak file and spin identification file, which then allow the detection of all possible proton–proton interactions contained in NOE cross-peaks. Analyzing such a proton–proton interaction list based on combined 2D and 3D NMR data permits the assignment of 99% of the protons and a large number of sequential and remote distance connectivities.

3D proton NMR has been shown to be a useful tool for resolving ambiguities arising from 2D data sets. A unique feature of the 3D spectrum is that the overlapped cross-peaks can be identified by not only the chemical shift differences, which to a certain extent also can be achieved by using 2D data sets, but also the spin transfer order differences. A systematic approach for analyzing overlapped HN/Hα cross-peaks in apo-NCS has been demonstrated. We stress the importance of combined utilization of 2D and 3D NMR data, since there are some experimental and theoretical limitations for 3D NMR experiments.

We have obtained 1270 nonfixed proton–proton distances from the apo-NCS NOE analysis, which forms a basis for the high-resolution solution structural determination by restrained molecular dynamics and/or distance geometry computations. The structure refinement of apo-NCS based on NMR-determined distances, torsional angles, and stereospecific assignments is underway. Detailed conformational and structural features will be reported in the near future. Such results should provide bases for further studies of holo-NCS and other holoproteins in the NCS antitumor protein family.

Acknowledgments

Protein samples were obtained from Professor I. Goldberg at Harvard University (apo-NCS) and the Drug Synthesis and Chemistry Branch, Division of Cancer Treatment, National Cancer Institute (MMC). X. Gao thanks Dr. Peter Jeffs for his support and critical manuscript reading and Professor Goldberg for helpful discussions. Amino acid analysis of apo-NCS and apo-MMC was carried out by Nora Geddie (Glaxo). The initiation of this project was supported by a Leukemia Society Special Fellowship to X. Gao.

Supplementary Material Available

Six figures showing expanded NOESY plots for apo-NCS and apo-MMC, expanded DQ-COSY and DQF-COSY spectra, expanded NOESY plots recorded in H_2O with a presaturation pulse or a J–R pulse sequence, the secondary structure of apo-NCS, the two-dimensional alignment of seven antiparallel β-sheets in apo-NCS, and overlay NOESY plots covering the fingerprint region from two experiments differing in conditions by 0.4 pH unit and two tables giving chemical shifts of apo-NCS and sequential NOE assignments of apo-NCS (15 pages). Ordering information is given on any current masthead page.

References

Adjadj, É., Mispelter, J., Quiniou, É., Dimicoli, J.-L., Favadon, V., & Lhoste, J.-M. (1990) *Eur. J. Biochem. 190*, 263–271.

Breg, J. N., Boelens, R., Vuister, G. W., & Kaptein, R. (1990) *J. Magn. Reson. 87*, 646–651.

Feisk, S. W., & Zuiderweg, E. R. (1990) *Q. Rev. Biophys. 23*, 97–131.

Gilson, B. W., Herlihy, W. C., Samy, T. S. A., Hahm, K.-S., Maeda, H., Meienhofer, J., & Biemann, K. (1984) *J. Biol. Chem. 259*, 10801–10806.

Goldberg, I. H. (1986) in *Molecular Mechanisms of Carcinogenic and Antitumor Activity* (Chagas, C., & Pullman, B., Eds.) pp 425–489, Aedibus Academicis: Civitate Vaticana.

Griesinger, C., Sørensen, O. W., & Ernst, R. R. (1987) *J. Am. Chem. Soc. 109*, 7227–7228.

Griesinger, C., Sørensen, O. W., & Ernst, R. R. (1989) *J. Magn. Reson. 84*, 14–63.

Ishida, N., Miyazaki, K., Kumaigai, K., & Rikimaru, M. (1965) *J. Antibiot. Ser. A. XVIII*, 68–76.

Jung, G., & Kohnlein, W. (1981) *Biochem. Biophys. Res. Commun. 98*, 176–183.

Kay, L. E., Clore, G. M., Bax, A., & Gronenborn, A. M. (1990) *Science 249*, 411–414.

Kuromizu, K., Tsunasawa, S., Maeda, H., Abe, O., & Sakiyama, F. (1986) *Arch. Biochem. Biophys. 246*, 199–205.

McBride, T. J., Axelrod, M., Cullen, W. P., Marsh, W. S., Sodano, C. S., & Rao, K. V. (1965) *Proc. Soc. Exp. Biol. Med. 130*, 1188–1190.

Montgomery, R., Shepherd, V. L., & Vandrê, D. D. (1981) in *Antitumor Compounds of Natural Origin: Chemistry and Biochemistry* (Aszalos, A., Ed.) Vol. I, pp 79–122, CRC Press, Orlando.

Myers, A. G., Proteau, P. J., & Handel, T. M. (1988) *J. Am. Chem. Soc. 110*, 7212–7214.

Naoi, N., Miwa, T., Okazaki, T., Watanabe, K., Takeuchi, T., & Umezawa, H. (1982) *J. Antibiot. 35*, 806–813.

Lee, S. H., & Goldberg, I. H. (1989) *Biochemistry 28*, 1019–1026.

Napier, M. A., Holmquist, B., Strydom, D. J., & Goldberg, I. H. (1979) *Biochem. Biophys. Res. Commun. 89*, 635–642.

Oschkinat, H., Cieslar, C., & Griesinger, C. (1990) *J. Magn. Reson. 86*, 453–469.

Padilla, A., Vuister, G. W., Boelens, R., Kleywegt, G. J., Cavê, A, Parello, J., & Kaptein, R. (1990) *J. Am. Chem. Soc. 112*, 5024–5030.

Pletnev, V. Z., Kuzin, A. P., Trakhanov, S. D., & Kostetsky, P. V. (1982) *Biopolymers 21*, 287–300.

Remerowski, M. L., Glaser, S. J., Sieker, L., Samy, T. S. A., & Drobny, G. P. (1990) *Biochemistry 29*, 8401–8409.

Roey, P. V., & Beerman, T. A. (1989) *Proc. Natl. Acad. Sci. U.S.A. 36*, 6587–6591.

Sieker, L. C., & Gnanarajah, G. G. (1988) *Proteins: Struct., Funct., Genet. 3*, 252–255.

Suzuki, H., Miura, K., Kumada, Y., Takeuchi, T., & Tanaka, N. (1980) *Biochem. Biophys. Res. Commun. 94*, 255–261.

Vuister, G. W., Boelens, R., & Kaptein, R. (1988) *J. Magn. Reson. 80*, 176–185.

Vuister, G. W., de Waard, P., Boelens, R., Vliegenthart, J. F. G., & Kaptein, R. (1989) *J. Am. Chem. Soc. 111*, 772–774.

Vuister, G. W., Boelens, R., Padilla, A., Kleywegt, P. G., & Kaptein, R. (1990) *Biochemistry 29*, 1829–1839.

Wüthrich, K. (1986) *NMR of Proteins and Nucleic Acids*, John Wiley & Sons, New York.